A Mechanistic Study of the Brønsted-Acid Catalysis of *n*-Hexane → Propane + Propene, Featuring Carbonium Ions

Ken C. Hunter, Christa Seitz, and Allan L. L. East*

Department of Chemistry and Biochemistry, University of Regina, Regina, Saskatchewan S4S 0A2, Canada

Received: August 14, 2002; In Final Form: October 22, 2002

A hypothetical five-step catalytic cycle for Brønsted-mediated fission of an all-trans *n*-alkane was examined using density functional theory. Optimized geometries and transition states were determined for catalyst−reactant complexes, using three different monodentate catalyst ions (NH_4^+, H_3O^+, and H_2F^+). Despite the wide variety of catalyst acidities, protonated hexane appears as an intermediate (not a transition state) in each case. The protonated cyclopropane structure is the most likely initial form of the dissociated product ion. The predicted intermediates were seen to vary with catalyst acidity. The complete energy profiles of this model catalytic cycle are provided and fitted to a cosine expansion, which allows for generation of the energy profile for any Brønsted catalyst and any *n*-alkane only on the basis of the proton affinities of the *n*-alkane and the conjugate base of the catalyst. Remarks on the applicability to zeolites and ionic liquid catalysts are given.

Introduction

Advances in computer modeling and in spectroscopic detection of transient intermediates are making inroads into the understanding of many complex reaction mechanisms. One such field is petroleum modification. There is much interest in the design and testing of new catalysts for acid-catalyzed cracking of hydrocarbons into smaller, more useful fragments. While current industrial processes use zeolites as their catalysts of choice, research is ongoing with other possibilities, including newer zeolites, other molecular sieves, and ionic liquids.

Many of the steps in the chemical mechanisms for acid-catalyzed alkane cracking are understood in a general sense, but some of the details are still unknown. For instance, a monomolecular β-scission rule for carbenium ions (acyclic $C_xH_{2x+1}^+$) and alkyl radicals (acyclic C_xH_{2x+1}) is well-known and generally accounts for most of the C−C-bond cracking.[1,2] However, the initiation steps whereby these ions and radicals are first created are still under debate and may vary for different catalysts.[3−11] Another example is in generalized reaction schemes, such as the excellent one of Cortright et al.[12] for acid-catalyzed cracking of alkanes involving several catalytic cycles, which we reproduce here in Figure 1. The circled ions are assumed to reside at the catalyst surface (hence, H^+ refers to the activated Brønsted catalyst). This generalized scheme omits the fine details along the reaction paths, and of particular interest to us are the possible intermediates in the initiation reaction $H^+ + C_x \rightarrow C_{x-y} + C_y^+$.

Carbonium ions (protonated alkanes, acyclic $C_xH_{2x+3}^+$) are gas-phase ions of very short lifetimes, originally detected and studied via mass spectrometry experiments.[13−24] Only two gas-phase infrared spectra have been reported to date.[25,26] Solution-phase carbonium ions have never been directly detected, although one was first proposed[27] in 1952 and the idea has been greatly popularized by Olah, following his initial reactions of alkanes with superacids,[2,28−30] and by Haag and Dessau, who incorporated them into catalytic cracking mechanisms.[5,31] Many theoretical chemistry studies of these intermediates have appeared; the ones since 1997 have studied these species either in isolation[32−45] or in contact with small catalyst models.[46−60]

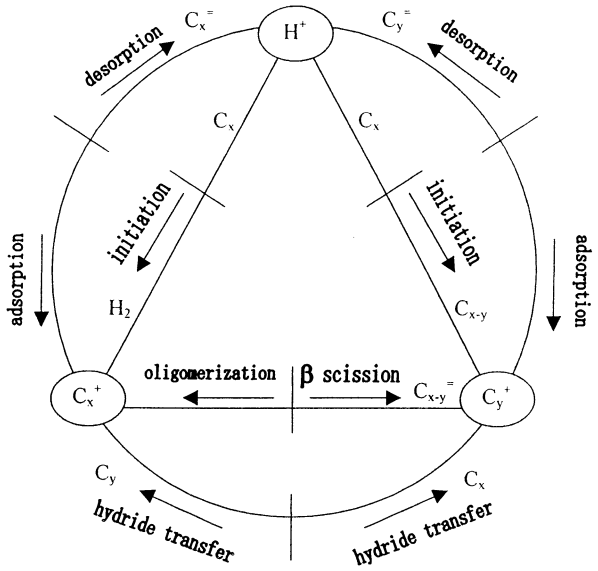

Figure 1. Generalized reaction scheme for Brønsted-acid cracking of hydrocarbons (reproduced from ref 3, with permission). Species C_x^+ and C_y^+ represent carbenium ions having *x* and *y* carbon atoms, respectively, with $x > y + 3$; C_x and $C_x^=$ represent alkanes and alkenes, respectively. The upper right cycle between H^+ and C_y^+ is under study here.

Theoretical simulations of alkane reactions involving carbonium ions have been reviewed recently,[61−63] but the current theoretical knowledge of the $H^+ + C_x \rightarrow C_{x-y} + C_y^+$ reaction mechanism is still significantly inadequate. The reasons for this are numerous: (i) the catalyst models suffer from omission of long-range effects;[59,60] (ii) most models investigate reactions of very small alkanes (butane or smaller), which either have abnormally low proton affinities[64,65] or the inability to generate the more ubiquitous "protonated cyclopropane" carbenium ion;[3,8] (iii) general conclusions are attempted on the basis of studies of catalysts of a very narrow acidity range; (iv) studies have typically been on individual steps, leaving it quite difficult to understand the full mechanism and thermodynamics of a

10.1021/jp021881u CCC: $25.00
Published on Web 12/10/2002

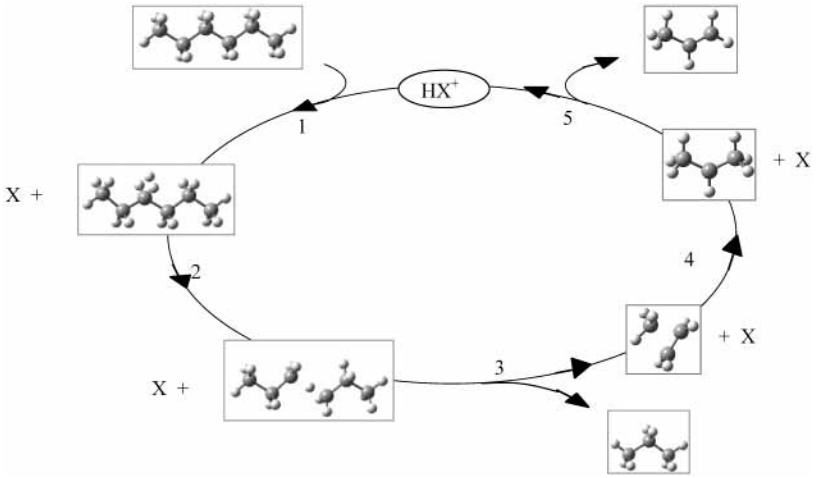

Figure 2. Our hypothetical five-step catalytic cycle for hexane → propane + propene. Steps 1 and 5 are proton-transfer ones, steps 2 and 4 are isomerizations, and step 3 is the cracking step.

catalytic cycle; (v) computations of transitions states involving complexes are difficult, and such results are still rare.

In this work, we undertook a project that makes inroads into points ii−v. We investigated one of the catalytic cycles described in Figure 1, namely, the cracking of *n*-hexane to propane and propene, where $x = 6$, $y = 3$, and the cycle occurs in the top right of Figure 1 between H^+ and C_3^+. We set up a hypothetical reaction mechanism featuring complexes with the catalyst and searched for transitions states at each step. Considering the known difficulties in modeling catalysts and the difficulties in optimizing transition states involving complexes, we chose to examine a fundamental trend (variations with catalyst acidity) with very simple models of Brønsted catalysts HX^+ (H_2F^+, H_3O^+, and H_4N^+). These Brønsted cations have conjugate-base proton affinities of 115.7, 164.5, and 204.0 kcal mol^{-1}, respectively, at 298 K.[66] This range contains the range of proton affinities of alkanes (140−170 kcal mol^{-1}, the proton affinity for the central bond in hexane being 160.7 kcal mol^{-1}),[65] and the results will therefore cover a great span of cases. The Brønsted-acid catalyst was chosen to be charged (e.g., $H_3O^+ \rightarrow H^+ + H_2O$) rather than neutral (e.g., $H_2O \rightarrow H^+ + OH^-$) to avoid steps that create charge separation because such steps might be adversely affected by the lack of complete solvation in the model; we plan to contrast the use of a neutral acid catalyst model in future work.

Catalytic reactions of hexane have been experimentally studied. Kung and co-workers[67] investigated the cracking of hexane with H-USY zeolite at 673 K and found that initially a non-β-scission mechanism operated, the two largest product fractions being propene (41%) and butene (20%). Other groups examined hexane cracking over other zeolites,[68−70] and variations in product distributions were noted, although propene was the most prevalent product in the initial reaction stages. We chose to investigate the most likely cycle to be operating in the initial reaction stages.

Figure 2 shows the hypothetical five-step catalytic cycle that we investigated, written counterclockwise as in Figure 1. In the first step, we imagine the HX^+ catalyst transferring the Brønsted proton to a sterically accessible σ_{CH} bond of the hexane, generating a hexonium ion with a CHH three-center−two-electron (3c2e) bond; we denote this isomer as $(ch)C_6H_{15}^+$. In the second step, the $(ch)C_6H_{15}^+$ ion isomerizes to a lower-energy $(cc)C_6H_{15}^+$ ion, featuring a CHC 3c2e bond. In the third step, the $(cc)C_6H_{15}^+$ ion dissociates to produce propane and a "primary propenium ion" (protonated cyclopropane). In the fourth step, we imagine the "primary propenium ion" ($p\text{-}C_3H_7^+$) would preferentially isomerize to the lower-energy secondary propenium ion ($s\text{-}C_3H_7^+$). In the fifth step, the secondary propenium ion back-transfers H^+ to regenerate the catalyst and produce propene. In our plots of the energy profile (PES or potential energy surface), we will add elementary zeroth and sixth steps: the initial complexation of the catalyst with hexane and the final decomplexation of the catalyst from the products.

Theoretical Methods

All calculations were performed with the software suite Gaussian 98, its 6-31G(d,p) basis set,[71] and the semiempirical density functional theory (DFT) model called B3LYP.[72,73] Molecular geometries and harmonic frequencies were computed using analytic first and second derivative formulas as is routine with Gaussian 98. The energies reported are not corrected for zero-point vibrational energies or thermal corrections, primarily because we are interested in the pure PES for the multistep reaction.

Transition-state optimizations involving complexes are quite difficult, and such results are still very rare in the literature. The prime difficulty is in avoiding convergence onto transition states for the rotation of one molecule relative to the other in the complex. Other difficult aspects were in trying to start in the correct neighborhood of coordinate space (where only one normal mode force constant is negative) and in dealing with particular reaction steps that involved multiple nonconcerted atomic motion. The most effective algorithm for us was the eigenvalue-following technique of Baker,[74] although we also relied on linear and quadratic synchronous transit, chemical intuition, and even trial-and-error to begin the algorithms in appropriate neighborhoods.

In several cases, particularly in the second half of the reaction cycle, animation of the imaginary frequency of a converged transition state was *not* sufficient evidence that we had obtained the transition state of interest, and therefore, we verified each transition state by either following the steepest-descent path or performing regular geometry optimizations on either side of the transition state until two minima were found and hence connected.

Complexes of two or three polyatomic molecules will often have several minima on the potential energy surface that differ primarily in relative orientation. In several instances, we attempted three or four different optimizations of the same

complex, and we relied on their graphical images and relative energies when choosing which converged minimum-energy structure had the most relevance to our chosen reaction cycle. We aimed to find a complete set of connected minima that would arise from the reaction of an all-trans *n*-hexane with the small catalyst molecule situated above the approximate plane of the carbon atoms. This did not always result in choosing the lowest-energy minimum for each intermediate complex; however, it did result in a connected reaction path, and the energetic effects of this choice were normally quite minor on the scale of the overall reaction-energy profile.

We did some brief calculations to estimate the accuracy of the B3LYP/6-31G(d,p) level of theory for this project. To estimate the magnitude of basis-set-superposition error for the dissociation $H_3O^+ \cdot C_6H_{14} \rightarrow H_3O^+ + C_6H_{14}$, we computed the energy of the products three ways: (i) the regular way with individually optimized geometries, (ii) the regular way but with the fragment geometry taken from the dimer geometry, and (iii) with basis functions of the missing monomer present and using the dimer geometry. The respective dissociation energies were 13.5, 16.7, and 16.0 kcal mol^{-1}. We computed zero-point and thermal (298 K) energy corrections for the complexes along the H_3O^+-catalyzed cycle, and the curve shifts uniformly except for the first two points ($H_3O^+ + C_6H_{14}$ and $H_3O^+ \cdot C_6H_{14}$), which would shift roughly 5 kcal mol^{-1} higher. We also used the coupled cluster method[75−77] for high-level CCSD(T)/cc-pVTZ//B3LYP/6-31G(d,p) energies for the activation energy for $H_2O \cdot p\text{-}C_3H_7^+ \rightarrow H_2O \cdot s\text{-}C_3H_7^+$, and the value of 14.1 kcal mol^{-1} is 4.0 kcal mol^{-1} higher than our B3LYP value. Therefore, we assess an accuracy of 5−10 kcal mol^{-1} for our results.

Results

Geometries and Energies Using Uncomplexed Species. Figure 2 presents images of the hydrocarbon species when optimized in isolation. In this study, an all-trans carbon chain was chosen for hexane and the hexonium ions. For the (ch)-$C_6H_{15}^+$ ion, the three-center−two-electron (3c2e) CHH bond includes a central carbon with the plane of this bond eclipsing the other CH bond and has the following specifics: $R_{HH} = 0.834$ Å, $R_{CH} = 1.340$ and 1.310 Å, $\theta_{HCH} = 37°$. For the (cc)$C_6H_{15}^+$ ion (C_2 point-group symmetry), the 3c2e CHC bond plane contains the C_2 symmetry axis and has the following specifics: $R_{CC} = 2.470$ Å, $R_{CH} = 1.265$ Å, $\theta_{CHC} = 157°$. For the carbenium ions, the isomer that would first result from dissociation of an all-trans *n*-carbonium ion would be a "primary carbenium ion," but it has long been known to have the appearance of a protonated cyclopropane (C_s symmetry);[78] at our level of theory, the three C−C bond distances are 1.394, 1.716, and 1.835 Å. The secondary propenium ion is of more traditional form with the methyl groups staggered with the secondary CH bond (although slightly disrotated with respect to each other, giving overall C_2 symmetry). A more detailed description of the isolated species can be found in our previous work.[65]

Figure 3 plots the relative energies of the catalytic cycle at each step computed using only isolated (uncomplexed) species. The overall reaction energy, $\Delta E = 20.8$ kcal mol^{-1}, compares rather well with the value obtained from heats of formation ($\Delta H_{298K} = 19.8$ kcal mol^{-1}).[79] The points are connected as if no activation barriers exist, which is certainly not the case—activation barriers cannot be provided in Figure 3 because the transition states for the proton-transfer steps (1 and 5) cannot be obtained with the catalyst and reactant in isolation.

The intercurve differences are due solely to the differences in acidity of the catalysts (or, said another way, the differences in proton affinity of the deprotonated catalysts); the weakly acidic NH_4^+ ion requires a very endothermic first step, while the strongly acidic H_2F^+ ion provides a very exothermic first step. Hence, our choice of catalysts should result in a broad range of energy-profile features for this reaction. The results within each given curve demonstrate that the (cc)$C_6H_{15}^+$ ion is a lower-energy isomer than the (ch)$C_6H_{15}^+$ ion, the intrinsic dissociation energy of (cc)$C_6H_{15}^+$ is only 10.6 kcal mol^{-1}, and the secondary propenium ion is a lower-energy isomer than protonated cyclopropane.

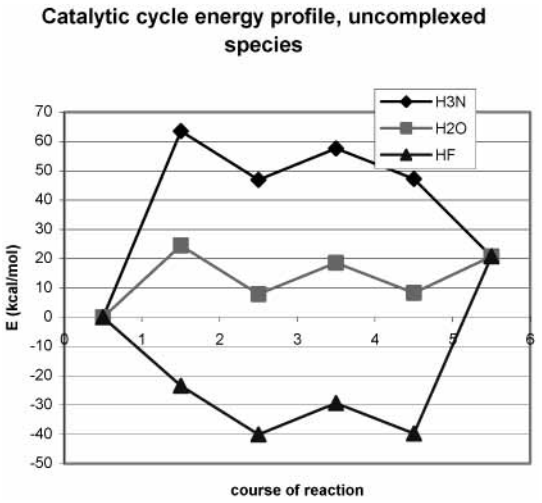

Figure 3. Energy profile for the catalytic cycle using uncomplexed species and using NH_4^+, H_3O^+, and H_2F^+ as Brønsted acids.

Geometries Using Complexed Species: Steps 1−3. In this section, we will present and discuss images of the minima and transition states for the first half of the catalytic cycle, leading up to the triple complex $X \cdot p\text{-}C_3H_7^+ \cdot C_3H_8$. Images of the optimized structures appear in Figure 4. Table 1 lists the relevant geometrical data from these structures, and Figure 5 is a sketch of the system to indicate which carbon and hydrogen atoms we call C_a, C_b, H_a, and H_b. Our hypothetical reaction path for these steps differs from Boronat et al.,[53] who envisaged a "billiard ball" reaction in which hydrogen H_a, rather than H_b, became the bridging proton. Both pathways are likely possible. Our hypothesis also differs from most, which imagine direct protonation of a C−C bond without participation of a CHH-carbonium ion isomer; in this case, our B3LYP results will be seen to support this alternative hypothesis for Brønsted catalysts having the acidity of H_3O^+ or lower.

The initial complex of the catalyst and hexane (denoted $HX^+ \cdot C_6H_{14}$) resulted in complexes in which a polar X−H_b bond (b for Brønsted) of the catalyst is "aimed" at a hexane CH_a bond (a for alkane). With the H_2F^+ catalyst, however, this minimum does not exist; in our attempts, a proton spontaneously transferred to the hexane without barrier. The second anticipated complex was that of deprotonated catalyst and a (ch)$C_6H_{15}^+$ ion, and in this system, the preferred minimum featured the negative end of the molecular dipole of HF aimed at one of the 3c2e H atoms. With the H_2O and NH_3 deprotonated catalysts, however, this minimum does not exist; in our attempts, a proton transferred back to the catalyst without barrier. Hence, only three of the first six hypothesized minima exist at the B3LYP/6-31G-(d,p) level of theory. These first three optimized structures appear in the first row of Figure 4.

An X·(cc)$C_6H_{15}^+$ complex is the next intermediate on the reaction path for all three catalysts. We chose the versions in which the deprotonated catalyst has its negative end aimed at the H atom of the CHC 3c2e bond because we are envisaging

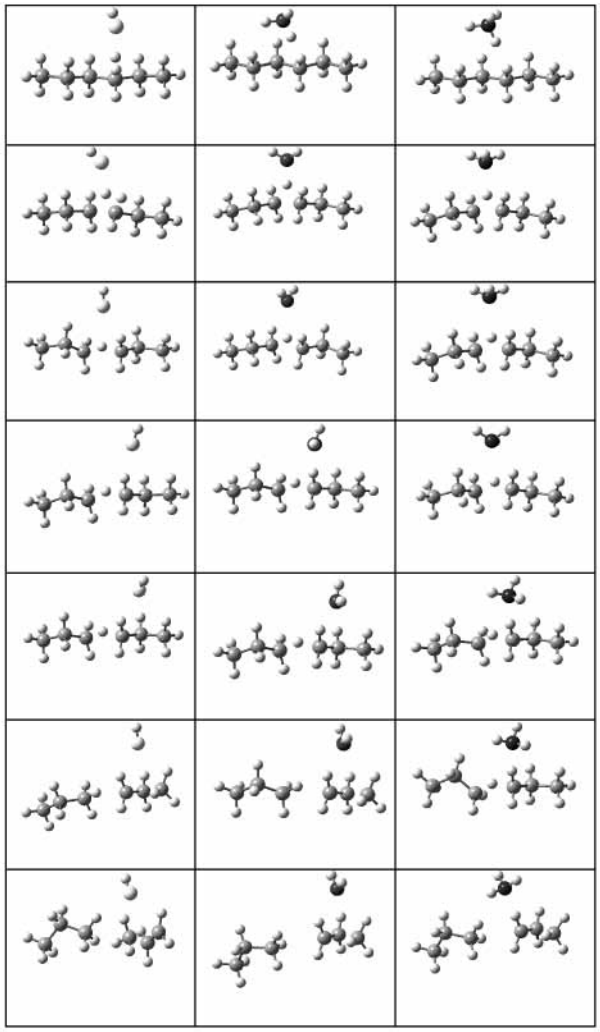

Figure 4. Images of optimized minima (rows 1, 3, 5, and 7) and transition states (rows 2, 4, and 6) for the first half of the catalytic cycle, up to production of propane: first column, H_2F^+ catalyst; second column, H_3O^+; third column, NH_4^+.

a reaction path in which the Brønsted proton becomes the CHC proton.

In the case of H_2F^+, the first transition state leads from HF·(ch)$C_6H_{15}^+$ to HF·(cc)$C_6H_{15}^+$. In this step, the paired hydrogens H_a and H_b (0.88 Å apart) begin to uncouple in the transition state (1.09 Å) before completely separating (1.71 Å) in the CHC-carbonium ion isomer. The C−C distance expands to welcome the H_b proton, from 1.53 to 1.67 Å in the transition state and finishing at 2.44 Å for the CHC-carbonium ion. The distance from H_b to the carbon C_a (to which it is bonded throughout this step) decreases from 1.31 to 1.18 Å in the transition state before rising to 1.26 Å in HF·(cc)$C_6H_{15}^+$. The deprotonated catalyst is coordinated to H_b throughout, but the distance expands significantly (from 1.64 to 1.75 to 2.43 Å). The imaginary frequency (692*i* cm^{-1}) of the transition state corresponds to a vibrational mode in which H_b migrates between the C_aH_a and C_aC_b bonds.

The first transition state in the H_3O^+ and NH_4^+ cases differ from that of H_2F^+ because the first complex is HX^+·C_6H_{14}, and the first step leads directly to X·(cc)$C_6H_{15}^+$ with no X·(ch)-$C_6H_{15}^+$ minimum existing at our level of theory. In this first step, a proton-transfer step, the H_bX distance expands from 1.03 to 1.45 Å (transition state) to 2.31 Å in the H_3O^+ case and from 1.04 to 1.89 to 2.32 Å in the NH_4^+ case. The transition state is much later in the NH_4^+ case than the H_3O^+ case because the reaction step is much more endothermic (41 vs 9 kcal mol^{-1}). The C−C distance increases from 1.54 to 1.71 to 2.26 Å in the H_3O^+ case and from 1.54 to 1.87 to 2.12 Å in the NH_4^+ case. Note that the trends in the 3c2e bond geometry of X·(cc)$C_6H_{15}^+$ complexes (e.g., $R(C_aC_b) = 2.44$, 2.26, and 2.12 Å for HF, H_2O, and NH_3 complexes, respectively) can easily be explained by the proton affinity of the complexing molecules, which tug on the bridging H_b atom. The imaginary frequency of the H_3O^+ and NH_4^+ transition states (958*i* and 266*i* cm^{-1}, respectively) corresponds to a vibrational mode in which the proton migrates directly between the catalyst nucleophile and the center of the C_aC_b bond.

A second X·(cc)$C_6H_{15}^+$ complex turned out to be the next intermediate on our reaction path for all three catalysts. In these complexes, the catalyst molecule has its negative end pointed not to the bridging H_b but to the paraffinic hydrogen atoms, particularly H_a. The transition state for this hopping step from H_b to H_a was somewhat similar for all three catalysts but showed some differences. For instance, for NH_3 and HF, the $\phi(XC_aC_5C_6)$ dihedral angle takes on values of 122°−126° in the first minimum and 66°−68° in the second minimum and traverses the intermediate values fairly straightforwardly, but in the H_2O case, the path is very curved: this parameter first moves to 103° and an additional minimum before the water performs the hop with a dihedral angle of 67° for the transition state and 58° for the finishing value in the second (truly the third) minimum. This peculiarity may be related not just to the proton affinity of H_2O but also to its steric expanse because the number of atoms bonded to X (two for H_2O) may play a role in allowing H_2O to find this additional minimum in a steric crevasse during the hop. We chose not to include this additional minimum at $\phi(XC_aC_5C_6) = 103°$ in our tables and figures.

Note also that during this hopping step, the $\theta(C_aH_bC_b)$ angle of the 3c2e bond increases to a more consistent value (141°−150° instead of 115°−152°) because of the lowered effect of the nucleophile upon the bridging proton.

The next step in the cycle is the dissociation or cracking step, from X·(cc)$C_6H_{15}^+$ to the "triple complex" X·p-$C_3H_7^+$·C_3H_8. We have found optimized triple complexes for each catalyst, in which the propenium ion adopts a protonated cyclopropane structure (as in the isolated-species optimization and which we denoted as p-$C_3H_7^+$ for primary propenium ion) and the catalyst molecule stays above the ring of the developing $C_3H_7^+$ unit. In the NH_3 triple complex, the dipole axis of the deprotonated catalyst is collinear with a CH bond of the propenium ion, while in the HF case, it is aimed at the center of the cyclopropane ring, and in the H_2O case, it lies somewhat between these cases.

The transition states for this cracking step have imaginary frequencies of 160*i*, 152*i*, and 124*i* cm^{-1} for the HF, H_2O, and NH_3 complexes, respectively. This mode involves primarily motion of the fourth carbon (C_a) that oscillates between creating a C_b-C_a bond or a $C_a-C_5-C_6$ protonated cyclopropane structure. In addition to this C_a motion, the reaction path also features a terminal methyl twist in the developing propenium unit and a twist of the dissociating carbon chains. The C_aC_b bond distances expand from 2.4 to 2.9 Å in the transition state and 3.2 Å in the resulting triple complex and are roughly 0.04 Å smaller with the NH_3 catalyst than with the other two. The CH_bC angles in the transition state (141°, 145°, and 148° for NH_3, H_2O, and HF, respectively) do not change much from their values in the hexonium ion (141°, 146°, 150°) but are more contracted in the triple complex once this 3c2e bond is fully broken (114°, 111°, 110°). The cyclization of the developing propenium ion is best seen in its C−C−C angle ($C_aC_5C_6$), which

TABLE 1: B3LYP Optimized Geometrical Parameters along the First Half of the Catalytic Cycle[a]

$X = NH_3$

	$HX^+{\cdot}C_6H_{14}$	TS	first $X{\cdot}(cc)C_6H_{15}^+$	TS	second $X{\cdot}(cc)C_6H_{15}^+$	TS	$X{\cdot}C_3H_8{\cdot}p\text{-}C_3H_7^+$
$R(C_aC_b)$	1.536	1.874	2.122	2.284	2.382	2.889	3.214
$R(H_aH_b)$	1.675	1.561	1.618	1.618	1.723	2.099	2.545
$R(H_bX)$	1.039	1.888	2.322	2.738	3.484	3.429	3.445
$R(H_aX)$	2.710	2.562	2.737	2.368	2.024	1.971	1.969
$R(H_bC_b)$	2.600	1.309	1.259	1.232	1.226	1.119	1.101
$R(H_bC_a)$	2.375	1.309	1.260	1.278	1.300	1.933	2.596
$\theta(XH_bH_a)$	174.5	95.5	86.0	59.4	23.5	31.4	34.4
$\theta(C_aH_aH_b)$	115.2	55.8	51.0	52.0	49.0	65.9	80.1
$\theta(C_aH_bC_b)$	35.6	91.4	114.8	131.0	141.1	140.9	114.5
$\theta(C_aC_5C_6)$	113.5	110.3	108.9	107.6	106.9	85.7	76.1
$\varphi(XC_aC_bC_2)$	−81.4	−91.8	−90.1	−71.0	−46.7	−25.7	2.4
$\varphi(XC_aC_5C_6)$	101.6	119.3	122.5	105.5	68.1	83.7	91.9
$\varphi(C_2C_bC_aC_5)$	−177.7	171.9	176.3	176.1	−171.6	−149.0	−120.7

$X = H_2O$

	$HX^+{\cdot}C_6H_{14}$	TS	first $X{\cdot}(cc)C_6H_{15}^+$	TS	second $X{\cdot}(cc)C_6H_{15}^+$	TS	$X{\cdot}C_3H_8{\cdot}p\text{-}C_3H_7^+$
$R(C_aC_b)$	1.537	1.717	2.264	2.417	2.415	2.933	3.264
$R(H_aH_b)$	1.335	1.549	1.666	1.725	1.739	2.126	2.677
$R(H_bX)$	1.029	1.448	2.314	3.412	3.653	3.864	4.476
$R(H_aX)$	2.356	2.378	2.669	1.972	2.030	2.058	2.198
$R(H_bC_b)$	2.432	1.407	1.256	1.230	1.229	1.119	1.100
$R(H_bC_a)$	2.068	1.408	1.253	1.292	1.297	1.949	2.698
$\theta(XH_bH_a)$	170.7	105.0	82.5	24.3	15.4	22.2	21.0
$\theta(C_aH_aH_b)$	113.6	61.5	48.8	48.5	48.2	65.7	79.4
$\theta(C_aH_bC_b)$	38.9	75.2	128.9	146.8	145.8	144.6	111.4
$\theta(C_aC_5C_6)$	113.6	111.3	108.3	106.1	106.0	84.8	74.1
$\varphi(XC_aC_bC_2)$	−76.3	−96.9	−91.5	−48.0	−55.6	−54.8	−40.3
$\varphi(XC_aC_5C_6)$	96.7	117.1	125.6	66.8	57.6	68.8	74.5
$\varphi(C_2C_bC_aC_5)$	−178.3	170.2	−179.2	−170.1	−172.2	−157.0	−134.0

$X = HF$

	$X{\cdot}(ch)C_6H_{15}^+$	TS	first $X{\cdot}(cc)C_6H_{15}^+$	TS	second $X{\cdot}(cc)C_6H_{15}^+$	TS	$X{\cdot}C_3H_8{\cdot}p\text{-}C_3H_7^+$
$R(C_aC_b)$	1.533	1.668	2.440	2.424	2.440	2.923	3.256
$R(H_aH_b)$	0.876	1.093	1.713	1.716	1.737	2.095	2.642
$R(H_bX)$	1.644	1.747	2.430	3.074	3.555	3.833	4.487
$R(H_aX)$	2.453	2.332	2.620	2.162	2.108	2.216	2.311
$R(H_bC_b)$	2.138	1.633	1.254	1.240	1.239	1.121	1.100
$R(H_bC_a)$	1.310	1.181	1.260	1.282	1.287	1.909	2.710
$\theta(XH_bH_a)$	152.1	108.1	76.3	43.0	24.8	28.1	23.3
$\theta(C_aH_aH_b)$	73.5	63.4	47.2	48.3	47.7	65.0	81.8
$\theta(C_aH_bC_b)$	45.3	70.6	152.1	148.0	150.0	148.3	110.1
$\theta(C_aC_5C_6)$	113.8	113.1	107.8	106.6	106.4	85.0	73.3
$\varphi(XC_aC_bC_2)$	−90.4	−81.3	−73.0	−85.7	−71.3	−101.6	−56.4
$\varphi(XC_aC_5C_6)$	88.3	101.1	124.0	86.7	66.7	75.7	76.6
$\varphi(C_2C_bC_aC_5)$	−173.8	172.7	−150.4	−171.0	−167.6	176.4	−137.1

[a] Bond lengths in Å, angles in deg. See Figure 5 for atom labeling.

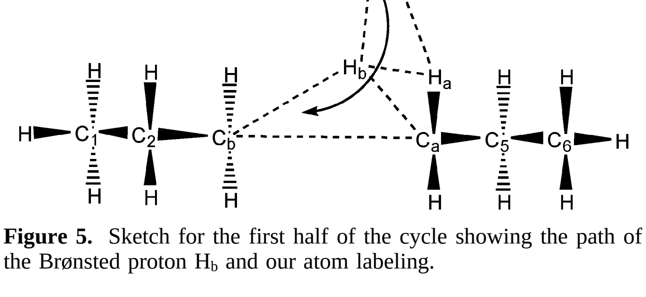

Figure 5. Sketch for the first half of the cycle showing the path of the Brønsted proton H_b and our atom labeling.

decreases from 106°−107° to 85°−86° in the transition state and 73°−76° in the dissociated triple complex. The twist of the dissociating carbon chain, from the all-trans form of the original hexane unit, causes 40°−60° changes in the ϕ-($C_5C_aC_bC_2$) dihedral angle, the values of which in the triple complex are −121°, −134°, and −137° for NH_3, H_2O, and HF, respectively. The values for $\phi(C_5C_aC_bC_2)$ in the transition state and triple complex are likely converged only to the nearest 5° because of the very flat potential surface for this parameter upon dissociation.

Geometries Using Complexed Species: Steps 4−5. The second half of the hypothesized catalytic cycle involves the conversion of $X{\cdot}p\text{-}C_3H_7^+$ to $HX^+{\cdot}C_3H_6$, with the omission of the propane that was produced from the previous step and is assumed to have left the complex. Images of the optimized structures appear in Figure 6. Table 2 lists the relevant geometrical data from our optimized structures for the minima and transition states, and Figure 7 is a sketch of the system to indicate the general reaction path as well as the atom labels used in Table 2.

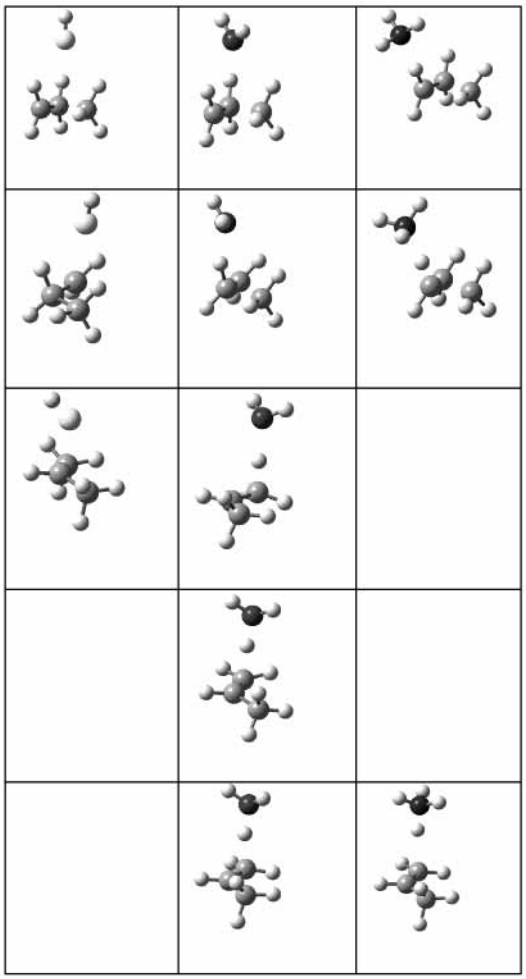

Figure 6. Images of optimized minima (rows 1, 3, and 5) and transition states (rows 2 and 4) for the second half of the catalytic cycle, after loss of propane: first column, H_2F^+ catalyst; second column, H_3O^+; third column, NH_4^+. Blank entries indicate the nonexistence of the corresponding stationary points.

For the X·p-$C_3H_7^+$ complexes in the absence of propane, the lowest-energy stable complexes featured the nucleophilic atom of the catalyst sitting coplanar with the carbon atoms of the primary propenium ion, rather than above the plane, and in the case of the NH_3 complex, the nucleophile actually strips H^+ from the propenium ion to leave a complex of NH_4^+ and cyclopropane. However, there were alternative minima in which the nucleophile is above the carbon plane, and these were chosen for our reaction profiles because they seem more directly accessible from the triple complex minima.

For the X·s-$C_3H_7^+$ complexes in the absence of propane, the results are varied. In the HF complex, the fluorine atom is strongly coordinated to the secondary carbon atom with a tight C−F interatomic distance of 2.1 Å. In the H_2O complex, the oxygen atom is coordinated to a H atom of a methyl group. In the NH_3 case, there is no such complex; optimizations resulted in proton transfer to create propene and NH_4^+.

The transition state for the isomerization of p-$C_3H_7^+$ to s-$C_3H_7^+$ was obtained many years ago by Schleyer and co-workers[78] and was found to look quite unexpected (no indication of the desired proton transfer) because of the numerous coordinate changes being nonconcerted in this reaction. We found the same thing in our complexed versions, except that we found *two* versions for the H_2O-catalyzed transition state. The higher-energy path, which we will ignore, involves CCC angle expansion and a rotation about the C_a-C_5 bond, followed by a 1,2-hydrogen shift from C_5 to C_a, with the catalyst continually complexed to a C_a hydrogen atom. The lower-energy path, shown in Figure 7 and common to all three catalysts, involves a methyl shift from C_5 to C_a, followed by CCC angle expansion and a rotation about the C_a-C_5 bond, and then followed by a 1,2-hydrogen shift from C_4 to C_5 (with the complexed catalyst in tow) and a rotation about the C_a-C_6 bond. Our animations of the imaginary frequency mode (333*i*, 329*i*, and 343*i* cm^{-1} for HF, H_2O, and NH_3, respectively) indicate that the transition state occurs during the methylene twist stage of this rather nonconcerted process. These transition states appear in the 2nd row of Figure 6. Note, however, that in the NH_3 case the transition state does not lead to a stable NH_3·s-$C_3H_7^+$ intermediate but to the NH_4^+·C_3H_6 product, which lies beyond (and at lower energy than) the NH_3·s-$C_3H_7^+$ configuration.

These internal coordinate changes for this isomerization path appear in the Table 2 data. The methyl shift can be seen in the

TABLE 2: B3LYP Optimized Geometrical Parameters along the Second Half of the Catalytic Cycle[a]

X = NH_3

	X·p-$C_3H_7^+$	TS	HX^+·C_3H_6
$R(H_cX)$	3.911	3.978	3.363
$R(H_aX)$	1.961	1.833	1.068
$R(H_aC_5)$	2.202	2.179	2.021
$R(C_aX)$	3.076	2.974	3.346
$R(C_5X)$	3.988	3.886	3.066
$R(C_aC_6)$	1.863	1.654	1.497
$R(C_5C_6)$	1.673	2.237	2.530
$\theta(C_5C_aC_6)$	59.7	94.1	125.6
$\theta(C_5C_aX)$	121.2	121.5	66.4
$\phi(H_aC_aC_5C_6)$	92.3	104.6	95.1
$\phi(H_cC_5C_aC_6)$	−103.4	−67.2	2.1
$\phi(H_dC_6C_aC_5)$	180.0	−162.0	128.6
$\phi(H_eC_aC_5C_6)$	−92.3	−115.6	−177.1

X = H_2O

	X·p-$C_3H_7^+$	TS	X·s-$C_3H_7^+$	TS	HX^+·C_3H_6
$R(H_cX)$	2.773	3.388	3.262	2.980	2.994
$R(H_aX)$	2.212	1.828	1.623	1.199	1.172
$R(H_aC_5)$	2.145	2.085	1.202	1.499	1.541
$R(C_aX)$	2.998	2.926	2.824	3.118	3.101
$R(C_5X)$	3.223	3.533	3.279	2.662	2.676
$R(C_aC_6)$	1.840	1.641	1.460	1.485	1.487
$R(C_5C_6)$	1.696	2.379	2.551	2.537	2.536
$\theta(C_5C_aC_6)$	61.4	102.8	126.0	125.8	125.8
$\theta(C_5C_aX)$	86.3	103.9	59.0	58.1	59.3
$\phi(H_aC_aC_5C_6)$	91.1	104.1	92.2	92.8	93.0
$\phi(H_cC_5C_aC_6)$	−100.4	−62.8	17.1	8.0	6.9
$\phi(H_dC_6C_aC_5)$	−175.3	−176.8	128.8	128.9	129.2
$\phi(H_eC_aC_5C_6)$	−95.1	−121.7	175.7	179.1	179.7

X = HF

	X·p-$C_3H_7^+$	TS	X·s-$C_3H_7^+$
$R(H_cX)$	2.352	2.195	2.978
$R(H_aX)$	2.319	2.289	2.854
$R(H_aC_5)$	2.147	1.973	1.092
$R(C_aX)$	2.943	2.958	2.116
$R(C_5X)$	2.943	2.858	2.744
$R(C_aC_6)$	1.831	1.606	1.458
$R(C_5C_6)$	1.718	2.506	2.575
$\theta(C_5C_aC_6)$	62.7	112.3	124.0
$\theta(C_5C_aX)$	76.3	72.1	98.6
$\phi(H_aC_aC_5C_6)$	92.4	105.1	162.2
$\phi(H_cC_5C_aC_6)$	−99.2	−52.9	−32.1
$\phi(H_dC_6C_aC_5)$	−175.2	172.6	156.9
$\phi(H_eC_aC_5C_6)$	−95.6	−132.0	−162.9

[a] Bond lengths in Å, angles in deg. See Figure 7 for atom labeling.

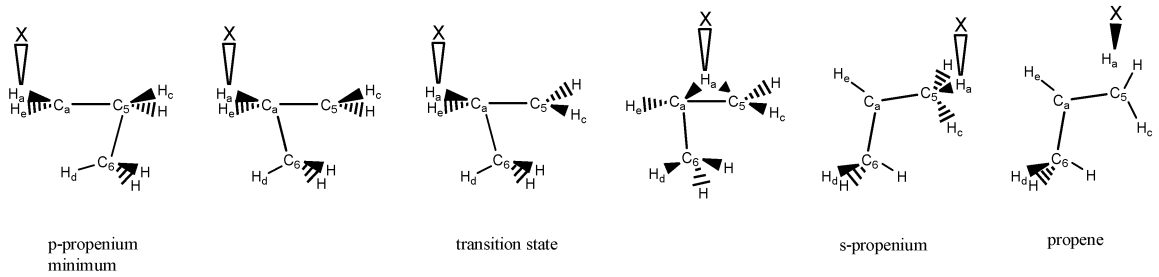

Figure 7. Sketch for the second half of the cycle showing the nonconcerted step 4 and simple step 5 and our atom labeling.

two listed CC bond distances, which show the methyl C_6 atom initially closer to carbon C_5 but then to carbon C_a at the first transition state and beyond. It can also be seen in $\theta(C_5C_aC_6)$, which is 60°−63° in the p-$C_3H_7^+$ complexes but 124°−126° in the s-$C_3H_7^+$ and C_3H_6 complexes. The methylene rotation at C_5 can be seen in the dihedral angle $H_cC_5C_aC_6$, which for the H_2O case varies from −100° to −63° (transition state) to 17° (X·s-$C_3H_7^+$). The shift of H_a from C_a to C_5 can be seen either in the H_aC_5 distance or in the C_5C_aX angle because the catalyst X transfers along with the H_a atom.

The final step of H^+ transfer back to the catalyst would hypothetically lead to a complex of HX^+ with propene. Optimizations of these HX^+·C_3H_6 structures succeeded for H_3O^+ and NH_4^+ but not H_2F^+ in which case H^+ back-transferred from the catalyst to the propene without barrier. The successful optimizations resulted in the catalyst positioned over the CH_2 carbon of the propene above the plane of the carbon atoms with the X−H bond aimed slightly to the middle of the double bond; the images of these structures appear in the fifth row of Figure 6. The final conceived transition state would be one for X·s-$C_3H_7^+$ → HX^+·C_3H_6, but such a transition state exists only for the H_2O complex. The reaction path involves a simple proton-transfer motion of H_a from C_5 to X but also an intriguing wag (inversion) of H_2O that occurs first. The transition state is very late, and animation of the imaginary frequency (179*i* cm^{-1}) shows only a proton-transfer motion. A perusal of the geometries in Table 2 demonstrates how closely this transition state resembles the geometry of the H_3O^+·C_3H_6 product.

We close this section with the comment that the complexation energies of carbocations with deprotonated catalyst are fairly consistent throughout the reaction and fairly independent of the catalyst. These average ion−molecule complexation energies were 14.6 ± 3.3 kcal/mol for HF, 15.3 ± 2.2 kcal/mol for H_2O, and 14.6 ± 4.8 kcal/mol for NH_3 complexes. The variance was greater for complexes of protonated catalysts with neutral hydrocarbons.

Energetics of the Catalytic Cycle with Complexed Species. The energies of the chosen conformers of the complexed species are listed in Table 3, and Figure 8 plots them versus course of reaction. The energies are connected with straight lines to mimic a crude potential energy surface for the catalytic cycle. Points that are unfilled and connected with dotted lines are points that do not represent stationary points and are given only as an approximate guide to the energy the system might have at that point on the reaction path; four of these points were guessed, and the remainder were estimated using the interval rule $[E(x;NH_3) - E(x;HF)]/[E(x;H_2O) - E(x;HF)] = {}^9/_5$ (on the basis of the locations of known points). This figure differs from Figure 3 (for uncomplexed species) in several important ways: transition-state energies are now able to be included, an extra hopping step for HX on (cc)$C_6H_{15}^+$ had to be added between steps 2 and 3, and a number of minima and transition states are now found not to exist. For the first half of the catalytic cycle (to

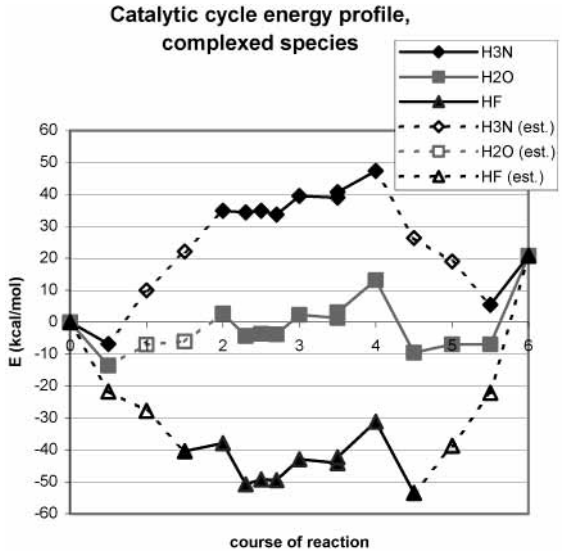

Figure 8. Energy profile for the catalytic cycle using complexed species and using NH_4^+, H_3O^+, and H_2F^+ as Brønsted acids. Open points and dotted lines represent estimated energies because no stationary points exist in these regions.

TABLE 3: Relative Energies (kcal mol^{-1}) at the B3LYP/6-31G(d,p) Level

compound	X = H_3N	X = H_2O	X = HF
$HX^+ + C_6H_{14}$	0.00	0.00	0.00
HX^+·C_6H_{14}	−6.85	−13.55	*a*
transition state	*a*	*a*	*a*
X·(ch)$C_6H_{15}^+$	*a*	*a*	−40.38
transition state	34.84	2.68	−37.86
X·(cc)$C_6H_{15}^+$ (1st)	34.35	−4.36	−50.77
transition state	34.89	−3.62	−49.23
X·(cc)$C_6H_{15}^+$ (2nd)	33.65	−3.79	−49.42
transition state	39.53	2.35	−42.96
X·p-$C_3H_7^+$·C_3H_8	38.95	1.36	−44.08
X·p-$C_3H_7^+ + C_3H_8$	40.74	3.09	−42.31
transition state	47.38	13.16	−31.19
X·s-$C_3H_7^+ + C_3H_8$	*a*	−9.59	−53.44
transition state	*a*	−6.98	*a*
HX^+·$C_3H_6 + C_3H_8$	5.39	−6.98	*a*
$HX^+ + C_3H_6 + C_6H_{14}$	20.76	20.76	20.76

[a] Not applicable.

point 3.5), the energy is given by the energy of the complete system, while for the second half (from point 3.5 on), the energy is computed by adding the energy of isolated propane to the energies of the system without propane. Hence, the vertical jump of 2 kcal mol^{-1} at point 3.5 is due to the loss of complexation energy caused by the removal of propane. The end points 0 and 6 are given by summing the energies of the isolated reactants (HX^+ and C_6H_{14}) and isolated products ($HX^+ + C_3H_8 + C_3H_6$).

Several points are worth noting. Within the limitations of the model, the plot shows that the (cc)$C_6H_{15}^+$ carbonium ion (at points 2.3 and 2.7 on the reaction path) is an intermediate, and

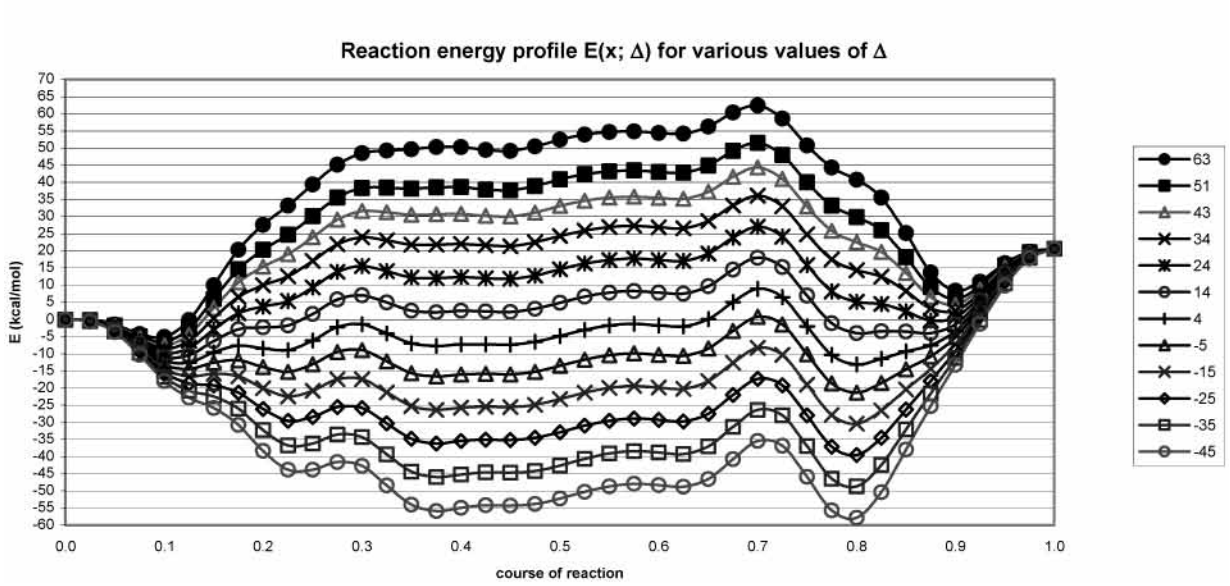

Figure 9. General energy profiles $E(x;\Delta)$ for the catalytic cycle for various values of Δ (the difference between the proton affinities of the catalyst conjugate base and the alkane). Note that the presence of certain intermediates depend crucially on the value of Δ for the system.

not a transition state, for the wide range of catalyst acidities tested here. This intermediate becomes more bound as the catalyst is made more acidic; for weak acids, the ion becomes prone to losing its extra proton back to the conjugate base of the catalyst. The (ch)$C_6H_{15}^+$ carbonium ion isomer will only exist in systems of exceptionally strong acidity. The cracking step (step 3) does have an associated transition state when in contact with a catalyst, unlike in the uncatalyzed gas-phase reaction. The most significant barrier in the overall reaction, other than the first step with NH_4^+ and the last step with H_2F^+, is, perhaps surprisingly, the isomerization of primary propenium ion (the protonated cyclopropane) to secondary propenium ion; our catalyzed activation barriers of 6−10 kcal mol^{-1} are in line with the uncatalyzed barrier of 13 kcal mol^{-1} from MP4/6-311G(d,p)//MP2/6-311G(d,p) calculations.[78] The proton exchange step from X·s-$C_3H_7^+$ to HX^+·C_3H_6 proceeds without any significant barrier, whether the reaction is exothermic, endothermic, or thermoneutral.

We wished to address the question of what the energy profile might look like for catalysts of other acidities and for other *n*-alkanes. We began with the hypothesis that these three energy profiles differ primarily because of one simple property, Δ, defined as the proton affinity of the conjugate base of the Brønsted-acid catalyst minus the proton affinity of the alkane. If we could find a functional form $E(x;\Delta)$ that could fit all three $E(x)$ curves with a simple change of the parameter value Δ, then we could use it to predict the $E(x)$ curve for any alkane and catalyst simply by computing their proton affinities.

The function that we ultimately chose is the cosine expansion

$$E(x;\Delta) = \sum_{0}^{18} C_n[\Delta] \cos(n\pi x)$$

where each coefficient C_n was considered to be a linear function of Δ. The argument of the cosine was taken so that the reaction coordinate x would vary from 0 to 1 with 1 representing the final products (point 6 in Figure 8). Two practical issues arose. The first was the ill-defined x values for points along the reaction path. For this issue, we assigned x values to each point using chemical intuition (such as incorporating early vs late transition-state locations) and continually adjusted them as suggested by some of the initial fitted curves. The second was the inability to determine 19 coefficients (required to accommodate some steep slopes in certain regions of the curve) from only 13 points or less along a given path. For this issue, we chose to connect the points of a given curve with a best-guess hand sketch, extract 41 points from this sketched curve, and then fit to these 41 points.

TABLE 4: Expressions for the Coefficients in the Potential Energy Function $E(x;\Delta)$ as Functions of the Proton Affinity Difference Parameter Δ (kcal mol^{-1})

coefficient	formula	coefficient	formula
C_0	$0.649\Delta - 5.88$	C_{10}	$0.041\Delta - 0.91$
C_1	$-0.070\Delta - 4.23$	C_{11}	$-0.014\Delta + 1.11$
C_2	$-0.467\Delta + 3.07$	C_{12}	$0.017\Delta + 0.73$
C_3	$0.009\Delta - 0.44$	C_{13}	$-0.008\Delta - 0.59$
C_4	$-0.191\Delta + 3.38$	C_{14}	$-0.016\Delta + 1.85$
C_5	$0.057\Delta - 3.96$	C_{15}	$0.008\Delta - 0.39$
C_6	$-0.042\Delta + 6.51$	C_{16}	$-0.006\Delta - 0.75$
C_7	$0.021\Delta - 1.86$	C_{17}	$0.008\Delta - 0.15$
C_8	$0.016\Delta + 3.34$	C_{18}	$-0.001\Delta - 1.06$
C_9	$-0.011\Delta + 0.22$		

The fitting process had two stages. In the first, we collected three sets of the 18 coefficients (one set for each catalyst) from the fits to the hand-sketched curves, using an iterative two-step process: a fit of 41 points was performed, followed by adjusting several of these 41 points as suggested by the fit, and repeating several times. The final curves fit all 123 finalized data points to within 0.3 kcal mol^{-1}. In the second stage, the coefficients from the first stage were resorted into 18 sets of three (one set for each C_n) and themselves subjected to linear fits versus B3LYP Δ values. Each coefficient produced very linear relationships with Δ, bolstering confidence in the method. The hand sketches introduce a source of bias to the procedure, while the linear fits of the resulting coefficients serve to remove a portion of this bias. From the second stage, the final fitted coefficients are listed in Table 4, and the proton affinities and Δ values are listed in Table 5; these two tables fully define our resulting predictive function $E(x;\Delta)$. Comparison of this function to our 123 finalized data points shows agreement to within 1 kcal mol^{-1} for all but two points (1.1 and 1.3 kcal mol^{-1} errors).

Figure 9 plots $E(x;\Delta)$ for 12 different values of Δ varying from −45 to +63 kcal mol^{-1}. From Table 5, the curves

TABLE 5: Proton Affinity Table (kcal mol^{-1})

compound	PA (actual)	Δ (actual)	Δ (B3LYP)
C_6H_{14}	160.7[a]		
NH_3	204.0[b]	43.3	46.9
H_2O	164.5[b]	3.8	7.9
HF	115.7[b]	−45.0	−40.0

[a] Reference 65. [b] Reference 66.

appropriate for NH_4^+, H_3O^+, and H_2F^+ are $\Delta = +43$, $+4$, and -45, respectively. Figure 9 is useful in two ways. First, it provides predictions for the complete reaction energy profile only on the basis of simple proton affinities. Second, it provides an elegant explanation as to why certain intermediates appear only with certain combinations of reactant and catalyst. For instance, the intrinsic proton-transfer barrier between $HX^+ \cdot C_nH_{2n+2}$ and $X \cdot (ch)C_nH_{2n+3}^+$ (at $x = 0.18$) is so small that these two complexes would coexist only over a narrow range of Δ cases (perhaps 0 to −10 kcal mol^{-1}), if at all, with only one of these two complexes existing in most Δ cases. The same appears to be true for the intrinsic barrier between $X \cdot s\text{-}C_{n/2}H_{n+1}^+$ and $HX^+ \cdot C_{n/2}H_n$ (at $x = 0.85$), the Δ value for coequilibrium being near +14 kcal mol^{-1}.

Finally, we would like to use our $E(x;\Delta)$ function to offer an explanation for the conflicting results of two recent theoretical studies that studied portions of this cycle with simple zeolite models. To do this, we computed the conjugate-base proton affinities of several small zeolite models, such as $HX^+ = [Al(OHSiH_3)_2(OH)_2]^+$, $[Al(OHSiH_3)_2(OSiH_3)_2]^+$, and $H_3SiOH-Al(OSiH_3)_2-O-Si-OH^+-Al(OSiH_3)_2-OHSiH_3$, and found them all to be 0−20 kcal mol^{-1} above the value for NH_3. This suggests that the curves for zeolite cracking of hexane might have the appearance of the top 3 curves in Figure 9.

Zygmunt et al.[59] modeled the cracking of ethane on substantially sized zeolite models and considered the end product to be methane and methoxyzeolite with no regeneration of catalyst. They determined a B3LYP/6-31G(d) barrier height of 69 kcal mol^{-1} for a small cluster, which they corrected to 54 kcal mol^{-1} after consideration of long-range and other effects. Using our model and proton affinities of 205 for $Al(OHSiH_3)(OSiH_3)_3$ and 142 for ethane,[65] we derive a Δ value of 63; this corresponds to our highest $E(x;\Delta)$ profile in Figure 9, except that one must only consider the profile up to $x = 0.60$ on the reaction coordinate because of the methyl cation generation. This profile gives a cracking barrier ($x = 0.57$) of roughly 60 kcal mol^{-1} relative to the complexed reactants. Boronat, Viruela, and Corma[53] modeled the cracking cycle of butane → ethane + ethene on a small zeolite model and with MP2/6-31G(d) found a CHC-butonium ion to be an intermediate roughly 60 kcal mol^{-1} above reactants and 35 kcal mol^{-1} above products. Using our model and proton affinities of 209 for our closest zeolite model $Al(OHSiH_3)(OSiH_3)(OH)_2$ and 158 for butane,[65] we derive a Δ value of 51; this corresponds to our second highest $E(x;\Delta)$ profile in Figure 9, except that one must ignore the profile between $x = 0.6$ and 0.8 because of the ethyl cation lacking a secondary isomer. This profile places the $(cc)C_4H_{11}^+$ intermediate at 45 kcal mol^{-1} above the complexed reactants and 32 kcal mol^{-1} above the complexed products.

The comparisons seem reasonable, considering the differences in models, although our reaction profiles contain more intermediates due in part to the consideration of a longer alkane. The surprise from Figure 9 in these comparisons, however, is that it appears to explain why Boronat and co-workers found a carbonium ion intermediate, while Zygmunt and co-workers (with correlated methods) did not; the first minimum for this intermediate near $x = 0.35$ disappears for $\Delta > 60$ kcal mol^{-1}. The second minimum for this intermediate, near $x = 0.45$, appears to remain, but the barrier is 1 kcal mol^{-1}, likely smaller than the accuracy of our extrapolation of $E(x;\Delta)$ to high Δ values. Because the use of long-range catalyst effects and alkanes larger than butane drives the value of Δ well below 60, we think that Figure 9 demonstrates that carbonium ions are in fact (very short-lived) intermediates, and not transition states, on the potential energy surface for zeolite catalysis.

Future work would be (1) to consider the effects of polydentate catalyst models, (2) to attempt similar calculations for side reactions of $C_3H_7^+$, and (3) to use better approximations to compute more accurate energies for each reaction step. Such studies are planned in our laboratory.

Conclusion

A hypothetical five-step catalytic cycle for Brønsted-mediated fission of a typical *n*-alkane (*n*-hexane) was examined using density functional theory. Minimizations and transitions states were determined for complexes of catalyst with reactant species, using three different monodentate catalyst ions (NH_4^+, H_3O^+, and H_2F^+). The complete energy profiles of this model catalytic cycle were provided and fitted to a cosine expansion, which allows for generation of the energy profile for any Brønsted catalyst and any *n*-alkane only on the basis of the difference, Δ, of proton affinities of the *n*-alkane and the conjugate base of the catalyst.

Within the limitations of the monodentate-catalyst model, protonated hexane appears as an intermediate (not a transition state) in each case, despite the wide variety of catalyst acidities. Other predicted intermediates were seen to vary with catalyst acidity, $(ch)C_6H_{15}^+$ (CH-protonated alkane) and $s\text{-}C_3H_7^+$ (secondary carbenium ion) appearing for only extremely acidic Brønsted catalysts. The cracking of an all-trans CC-protonated alkane ion likely leads to a protonated cyclopropane structure ($p\text{-}C_3H_7^+$), which is bound by 5−10 kcal mol^{-1} relative to conversion to secondary carbenium ions or alkenes. Based on the proton affinity of small zeolite models, the energy profiles most relevant for zeolite catalysts are the profiles for Δ values from 30 to 60 kcal mol^{-1}, and the resulting sizable activation energies (>40 kcal mol^{-1}) are in fair agreement with those of other researchers. Earlier zeolite-modeling studies, which predict carbonium ions to be transition states rather than intermediates, appear to have suffered from the use of very small alkanes, and our calculations suggest that minima do exist for complexes of carbonium ions with zeolites as well as ionic liquids.

Acknowledgment. The Institute of Computational Discovery (University of Regina) is thanked for computer time on the SGI Onyx 2 supercomputer. S. Hepperle is thanked for aid with least-squares fitting. NSERC (Canada) is thanked for research funds.

References and Notes

(1) Wojciechowski, B. W.; Corma, A. *Catalytic Cracking*: *Catalysts, Chemistry, and Kinetics*; Dekker: New York, 1986.
(2) Olah, G. A.; Molnár, A. *Hydrocarbon Chemistry*; Wiley: New York, 1995.
(3) Brouwer, D. M.; Hogeveen, H. *Progr. Phys. Org. Chem.* **1972**, *9*, 179.
(4) Olah, G. A.; Halpern, Y.; Shen, J.; Mo, Y. K. *J. Am. Chem. Soc.* **1973**, *95*, 4960.
(5) Haag, W. O.; Dessau, R. M. *Proc. 8th Int. Congr. Catal.* **1985**, *2*, 305.
(6) Scherzer, J. *Catal. Rev.-Sci. Eng.* **1989**, *31*, 215.
(7) Culmann, J.-C.; Sommer, J. *J. Am. Chem. Soc.* **1990**, *112*, 4057.
(8) Adeeva, V.; Liu, H.-Y.; Xu, B.-Q.; Sachtler, W. M. H. *Top. Catal.* **1998**, *6*, 61.

(9) Fărcaşiu, D. *Catal. Lett.* **2001**, *71*, 95.
(10) Fokin, A. A.; Shubina, T. E.; Gunchenko, P. A.; Isaev, S. D.; Yurchenko, A. G.; Schreiner, P. R. *J. Am. Chem. Soc.* **2002**, *124*, 10718.
(11) Fokin, A. A.; Schreiner, P. R. *Chem. Rev.* **2002**, *102*, 1551.
(12) Cortright, R. D.; Dumesic, J. A.; Madon, R. J. *Top. Catal.* **1997**, *4*, 15.
(13) Tal'roze, V. L.; Lyubimova, A. L. *Dokl. Akad. Nauk SSSR* **1952**, *86*, 909; *Chem. Abstr.* **1953**, *47*, 2590.
(14) Meisels, G. G.; Hamill, W. H.; Williams, R. R., Jr. *J. Chem. Phys.* **1956**, *25*, 790.
(15) Meisels, G. G.; Hamill, W. H.; Williams, R. R., Jr. *J. Phys. Chem.* **1957**, *61*, 1456.
(16) Wexler, S.; Jesse, N. *J. Am. Chem. Soc.* **1962**, *84*, 3425.
(17) Field, F. H.; Franklin, J. L.; Munson, M. S. B. *J. Am. Chem. Soc.* **1963**, *85*, 3575.
(18) Munson, M. S. B.; Franklin, J. L.; Field, F. H. *J. Phys. Chem.* **1964**, *68*, 3098.
(19) Abramson, F. P.; Futrell, J. H. *J. Chem. Phys.* **1966**, *45*, 1925.
(20) Ding, A.; Henglein, A.; Lacmann, K. *Z. Naturforsch.* **1968**, *23A*, 780.
(21) Herman, Z.; Hierl, P.; Lee, A.; Wolfgang, R. *J. Chem. Phys.* **1969**, *51*, 454.
(22) Huntress, W. T., Jr. *J. Chem. Phys.* **1972**, *56*, 5111.
(23) Weiner, J.; Smith, G. P. K.; Saunders, M.; Cross, R. J., Jr. *J. Am. Chem. Soc.* **1973**, *95*, 4115.
(24) Hiraoka, K.; Kebarle, P. *J. Am. Chem. Soc.* **1976**, *98*, 6119.
(25) Yeh, L. I.; Price, J. M.; Lee, Y. T. *J. Am. Chem. Soc.* **1989**, *111*, 5597.
(26) White, E. T.; Tang, J.; Oka, T. *Science* **1999**, *284*, 135.
(27) Winstein, S.; Trifan, D. *J. Am. Chem. Soc.* **1952**, *74*, 1147.
(28) Olah, G. A.; Prakash, G. K. S.; Sommer, J. *Superacids*; Wiley-Interscience: New York, 1985.
(29) Olah, G. A.; Prakash, G. K. S.; Williams, R. E.; Field, L. C.; Wade, K. *Hypercarbon Chemistry*; Wiley-Interscience: New York, 1987.
(30) Olah, G. A.; Farooq, O.; Prakash, G. K. S. *Activation and Functionalization of Alkanes*; John Wiley & Sons: New York, 1989.
(31) Kotrel, S.; Knözinger, H.; Gates, B. C. *Microporous Mesoporous Mater.* **2000**, *35*−*36*, 11.
(32) Frash, M. V.; Solkan, V. N.; Kazansky, V. B. *J. Chem. Soc., Faraday Trans.* **1997**, *93*, 515.
(33) Otto, A. H.; Prescher, D.; Gey, E.; Schrader, S. *J. Fluorine Chem.* **1997**, *82*, 55.
(34) Collins, S. J.; O'Malley, P. J. *Top. Catal.* **1998**, *6*, 151.
(35) Boronat, M.; Viruela, P.; Corma, A. *J. Phys. Chem. B* **1997**, *101*, 10069.
(36) Boronat, M.; Viruela, P.; Corma, A. *J. Phys. Chem. B* **1999**, *103*, 7809.
(37) Mota, C. J. A.; Esteves, P. M.; Ramírez-Solís, A.; Hernández-Lamoneda, R. *J. Am. Chem. Soc.* **1997**, *119*, 5193.
(38) Esteves, P. M.; Mota, C. J. A.; Ramírez-Solís, A.; Hernández-Lamoneda, R. *J. Am. Chem. Soc.* **1998**, *120*, 3213.
(39) Esteves, P. M.; Mota, C. J. A.; Ramírez-Solís, A.; Hernández-Lamoneda, R. *Top. Catal.* **1998**, *6*, 163.
(40) Esteves, P. M.; Alberto, G. G. P.; Ramírez-Solís, A.; Mota, C. J. A. *J. Phys. Chem. A* **2000**, *104*, 6233.
(41) Okulik, N.; Peruchena, N.; Esteves, P. M.; Mota, C.; Jubert, A. H. *J. Phys. Chem. A* **2000**, *104*, 7586.
(42) Esteves, P. M.; Alberto, G. G. P.; Ramírez-Solís, A.; Mota, C. J. A. *J. Phys. Chem. A* **2001**, *105*, 4308.
(43) Okulik, N. B.; Sosa, L. G.; Esteves, P. M.; Mota, C. J. A.; Jubert, A. H.; Peruchena, N. M. *J. Phys. Chem. A* **2002**, *106*, 1584.
(44) East, A. L. L.; Liu, Z. F.; McCague, C.; Cheng, K.; Tse, J. S. *J. Phys. Chem. A* **1998**, *102*, 10903.
(45) Seitz, C.; East, A. L. L. *J. Phys. Chem. A*, in press.
(46) Rigby, A. M.; Kramer, G. J.; van Santen, R. A. *J. Catal.* **1997**, *170*, 1.
(47) Blaszkowski, S. R.; van Santen, R. A. *Top. Catal.* **1997**, *4*, 145.
(48) Frash, M. V.; van Santen, R. A. *Top. Catal.* **1999**, *9*, 191.
(49) Kazansky, V. B. *Catal. Today* **1999**, *51*, 419.
(50) Khaliullin, R. Z.; Bell, A. T.; Kazansky, V. B. *J. Phys. Chem. A* **2001**, *105*, 10454.
(51) Chatterjee, A.; Iwasaki, T.; Ebina, T.; Tsuruya, H.; Kanougi, T.; Oumi, Y.; Kubo, M.; Miyamoto, A. *Proc. 12th Int. Zeolite Conf.* **1999**, *1*, 489.
(52) Boronat, M.; Viruela, P.; Corma, A. *J. Phys. Chem. A* **1998**, *102*, 9863.
(53) Boronat, M.; Viruela, P.; Corma, A. *Phys. Chem. Chem. Phys.* **2000**, *2*, 3327.
(54) Esteves, P. M.; Nascimento, M. A. C.; Mota, C. J. A. *J. Phys. Chem. B* **1999**, *103*, 10417.
(55) Esteves, P. M.; Alberto, G. G. P.; Ramírez-Solís, A.; Mota, C. J. A. *J. Am. Chem. Soc.* **1999**, *121*, 7345.
(56) Esteves, P. M.; Ramírez-Solís, A.; Mota, C. J. A. *J. Braz. Chem. Soc.* **2000**, *11*, 345.
(57) Esteves, P. M.; Ramírez-Solís, A.; Mota, C. J. A. *J. Phys. Chem. B* **2001**, *105*, 4331.
(58) Zygmunt, S. A.; Curtiss, L. A.; Iton, L. E. *Proc. 12th Int. Zeolite Conf.* **1999**, *1*, 333.
(59) Zygmunt, S. A.; Curtiss, L. A.; Zapol, P.; Iton, L. E. *J. Phys. Chem. B* **2000**, *104*, 1944.
(60) Ahlberg, P.; Karlsson, A.; Goeppert, A.; Nilsson Lill, S. O.; Dinér, P.; Sommer, J. *Chem.*−*Eur. J.* **2001**, *7*, 1936.
(61) Bates, S. P.; van Santen, R. A. *Adv. Catal.* **1998**, *42*, 1.
(62) Sommer, J.; Jost, R. *Pure Appl. Chem.* **2000**, *72*, 2309.
(63) Kissin, Y. V. *Catal. Rev.* **2001**, *43*, 85.
(64) Auroux, A.; Tuel, A.; Bandiera, J.; Ben Taarit, Y.; Guil, J. M. *Appl. Catal. A* **1993**, *93*, 181.
(65) Hunter, K. C.; East, A. L. L. *J. Phys. Chem. A* **2002**, *106*, 1346.
(66) East, A. L. L.; Smith, B. J.; Radom, L. *J. Am. Chem. Soc.* **1997**, *119*, 9014.
(67) Williams, B. A.; Ji, W.; Miller, J. T.; Snurr, R. Q.; Kung, H. H. *Appl. Catal. A* **2000**, *203*, 179.
(68) Kotrel, S.; Rosynek, M. P.; Lunsford, J. H. *J. Phys. Chem. B* **1999**, *103*, 818.
(69) Isernia, L.; Quesada, A.; Lujano, J.; Imbert, F. E. In *12th International Congress on Catalysis*; Corma, A., Melo, F. V., Mendioroz, S., Fierro, J. L. G., Eds.; Studies in Surface Science and Catalysis 130; Elsevier: Amsterdam, 2000; p 2483.
(70) Talukdar, A. K.; Bhattacharyya, K. G.; Baba, T.; Ono, Y. *Appl. Catal. A* **2001**, *213*, 239.
(71) Frisch, M. J.; Trucks, G. W.; Schlegel, H. B.; Scuseria, G. E.; Robb, M. A.; Cheeseman, J. R.; Zakrzewski, V. G.; Montgomery, J. A., Jr.; Stratmann, R. E.; Burant, J. C.; Dapprich, S.; Millam, J. M.; Daniels, A. D.; Kudin, K. N.; Strain, M. C.; Farkas, O.; Tomasi, J.; Barone, V.; Cossi, M.; Cammi, R.; Mennucci, B.; Pomelli, C.; Adamo, C.; Clifford, S.; Ochterski, J.; Petersson, G. A.; Ayala, P. Y.; Cui, Q.; Morokuma, K.; Malick, D. K.; Rabuck, A. D.; Raghavachari, K.; Foresman, J. B.; Cioslowski, J.; Ortiz, J. V.; Stefanov, B. B.; Liu, G.; Liashenko, A.; Piskorz, P.; Komaromi, I.; Gomperts, R.; Martin, R. L.; Fox, D. J.; Keith, T.; Al-Laham, M. A.; Peng, C. Y.; Nanayakkara, A.; Gonzalez, C.; Challacombe, M.; Gill, P. M. W.; Johnson, B. G.; Chen, W.; Wong, M. W.; Andres, J. L.; Head-Gordon, M.; Replogle, E. S.; Pople, J. A. *Gaussian 98*, revision A.9; Gaussian, Inc.: Pittsburgh, PA, 1998.
(72) Becke, A. D. *J. Chem. Phys.* **1993**, *98*, 5648.
(73) Lee, C.; Yang, W.; Parr, R. G. *Phys. Rev. B* **1988**, *37*, 785.
(74) Baker, J. *J. Comput. Chem.* **1986**, *7*, 385.
(75) Cizek, J. *Adv. Chem. Phys.* **1969**, *14*, 35.
(76) Pople, J. A.; Head-Gordon, M.; Raghavachari, K. *J. Chem. Phys.* **1987**, *87*, 5968.
(77) Bartlett, R. J. *J. Phys. Chem.* **1989**, *93*, 1697.
(78) Koch, W.; Liu, B.; Schleyer, P. v. R. *J. Am. Chem. Soc.* **1989**, *111*, 3479.
(79) Weast, R. C. *CRC Handbook of Chemistry and Physics*, 67th ed.; CRC Press: Boca Raton, FL, 1987.